



This is the accepted manuscript made available via CHORUS. The article has been published as:

Narrow bands in magnetic field and strong-coupling Hofstadter spectra

Xiaoyu Wang and Oskar Vafek

Phys. Rev. B **106**, L121111 — Published 21 September 2022

DOI: 10.1103/PhysRevB.106.L121111

Narrow bands in magnetic field and strong-coupling Hofstadter spectra

Xiaoyu Wang¹ and Oskar Vafek^{1,2,*}

 $^1National\ High\ Magnetic\ Field\ Laboratory,\ Tallahassee,\ Florida,\ 32310,\ USA$ $^2Department\ of\ Physics,\ Florida\ State\ University,\ Tallahassee,\ Florida\ 32306,\ USA$

We develop a new, efficient, and general method to determine the Hofstadter spectrum of isolated narrow bands. The method works for topological as well as for trivial narrow bands by projecting the zero **B**-field hybrid Wannier states – which are localized in one direction and Bloch extended in another direction – onto a representation of the magnetic translation group in the Landau gauge. We then apply this method to find, for the first time, the Hofstadter spectrum for the exact single particle charged excitations in the strong coupling limit of the magic angle twisted bilayer graphene at the charge neutrality point and at $|\nu|=2$ down to low magnetic fields when the flux through the moiré unit cell is only $\sim 1/25$ of the electronic flux quantum i.e. $\sim 1T$ at the first magic angle. The resulting spectra provide a means to investigate Landau quantization of the quasiparticles even if their dispersion is interaction induced.

The rise of moiré materials [1–16] has brought into focus the challenge to understand the physics of correlated narrow bands subject to quantizing magnetic field ${\bf B}$ [17–24]. Such narrow bands can be topologically nontrivial even at ${\bf B}=0$, as is the case for the magic angle twisted bilayer graphene (MATBG)[25–27]. Moreover, for a moiré period ~ 13 nm, as in MATBG, the magnetic flux through the unit cell, ϕ , can readily become comparable or even exceed the flux quantum $\phi_0=hc/e$ using existing high field magnets, so that the interplay of strong correlation and Hofstadter physics can be realized in a laboratory [15, 28–30].

The traditional way to determine the non-interacting Hofstadter spectrum in the MATBG is to minimally couple the magnetic vector potential A to the continuum Bistritzer-MacDonald (BM) Hamiltonian [31] and then to expand it in the Landau level (LL) basis [17–20]. Although this provides a reliable method, it requires a large upper cutoff on the LL index [19] in order to converge, particularly at low B, or close to simple rational values of $\phi/\phi_0 = p/q$ where the LL basis method becomes prohibitively computationally expensive. This is because many Landau quantized remote bands are kept together with the narrow bands of interest. Equivalently, at low B, the real space shape of the narrow band wavefunctions — with peaks in the local density of states at the moiré triangular lattice sites — is mainly determined by the interlayer tunneling $(w_{0,1})$ induced periodic potential and a superposition of a large number of LLs is needed in order to recover such real space structure. Open-momentum space method introduced in Ref. [22] takes advantage of the sparse BM Hamiltonian matrix at $\mathbf{B} \neq 0$, but faces difficulties in uniquely identifying and removing the spurious momentum edge states. Moreover, although Coulomb interaction does not have a big effect on the remote bands, it dominates the dynamics of partially filled narrow bands, which remain separated from the remote bands by a band gap even when $\mathbf{B} \neq 0$ (see Fig. 2(a)). If one is then interested in interaction induced phenomena within the resulting narrow bands a

more efficient method is desirable.

The new method introduced here avoids the mentioned difficulties. We illustrate it at low **B**, but it is readily generalizable to vicinity of simple fractions p/q. Thus, we first solve the $\mathbf{B} = 0$ problem using standard (efficient) methods and find the hybrid Wannier states (hWSs) for the $\mathbf{B} = 0$ narrow bands [27, 32–34]. Such states are exponentially localized in one direction and Bloch extended in another, say y-direction [33] (see Fig. 1). We stress that even if the band is topologically non-trivial, there is no obstruction to 1D exponential localization. The key insight is that at $\mathbf{B} \neq 0$, for the hWS centered at and near the origin, the Landau gauge vector potential $\mathbf{A} = Bx\hat{\mathbf{y}}$ can be treated perturbatively, because the region in real space where A is large gets suppressed by the exponential localization of the hWS (see Fig. 1). Moreover, the discrete translation symmetry along the y-direction used in constructing the hWSs is preserved by such A. Next, we generate the rest of the basis by projecting the hWSs centered at and near the origin onto a representation of the magnetic translation group (MTG). This gives two quantum numbers, $k_1 \in [0,1)$ and $k_2 \in [0,1/q)$, associated with magnetic translations by two non-collinear vectors \mathbf{L}_1 and $q\mathbf{L}_2$ (Fig. 1). States with different k_1 and k_2 are then guaranteed to be orthogonal. Because in the original ($\mathbf{B} = 0$) Brillouin zone k_2 belonged to a larger range [0,1), we generate q states for each starting hWS at the same $k_1 \in [0,1)$ and $k_2 \in [0,1/q)$ when $\mathbf{B} \neq 0$. Thus, for each $\mathbf{B} = 0$ narrow band (of which there are two per valley and spin in MATBG) and for each hWS center described by a discrete index n_0 , we have q states. The resulting states at the same $k_1 \in [0,1)$ and $k_2 \in [0,1/q)$ then typically are not orthogonal, but by adjusting the range of n_0 , the set of states can be readily made overcomplete and span the $\mathbf{B} \neq 0$ narrow band Hilbert space. A simple procedure involving diagonalization of the overlap matrix and keeping the 2q largest overlap eigenvalues (per spin and valley) is then applied to obtain 2q orthogonal states within the MATBG narrow bands at $\mathbf{B} \neq 0$. For MATBG and at low **B** we find that the largest 2q

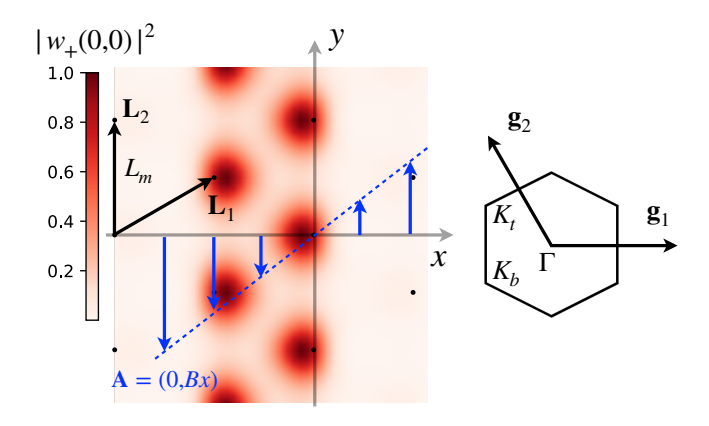


FIG. 1. Left: illustrative real space probability density of a hybrid Wannier state $|w_c(n_0, k_2\mathbf{g}_2)\rangle$, with Chern index c=+1, $n_0=0$ and $k_2=0$, and the Landau gauge magnetic vector potential $\mathbf{A}=Bx\hat{\mathbf{y}}$. Moiré unit cell primitive vectors are $\mathbf{L}_{1,2}$. Right: moiré Brillouin zone and reciprocal lattice vectors $\mathbf{g}_{1,2}$. $K_{t,b}$ denote the Dirac point from the top and bottom layers of the twisted bilayer graphene.

overlap eigenvalues are clearly separated by a gap from the remaining small eigenvalues, and that the 2q orthogonal states have an almost perfect support by the $\mathbf{B} \neq 0$ narrow bands only (see Fig. 2b and 2c).

If we use this method on a topologically trivial narrow band, then a single value of $n_0 = 0$ is sufficient and none of the overlap eigenvalues become small even when $\phi =$ ϕ_0 . On the other hand, for the topologically non-trivial narrow bands of MATBG, we need to keep at least two starting states with $n_0 = 0$ and $n_0 = \pm 1$ (for either sign) in order to obtain complete orthogonal basis spanning the $\mathbf{B} \neq 0$ narrow bands. This is a direct consequence of the non-trivial topology of the $\mathbf{B} = 0$ narrow band Hilbert space, spanned by a band with Chern number +1 and a band with Chern number -1, one of which is then deficient by p anomalous sub-bands while the other has an excess of p sub-bands when $\mathbf{B} \neq 0$ [35] [36–38]. We confirm this by studying the sublattice polarization of the resulting states in Fig. 3 and analytical arguments in the chiral limit presented in SM.

Our new basis can now be readily applied to finding the $\mathbf{B} \neq 0$ single electron or single hole excitation spectra in the strong coupling problem by using the method introduced in Refs. [39, 40]. Note that even at $\mathbf{B} \neq 0$, the 2-fold rotation about the out-of-plane axis C_2 , the particle-hole P [19, 27] and the valley U(1) conservation symmetries of the BM Hamiltonian are preserved at any w_0/w_1 ; the time reversal symmetry T is of course broken by \mathbf{B} . Therefore, C_2P guarantees that if $\Psi_{\mathbf{K},m,k_1,k_2}(\mathbf{r})$ is an eigenstate of $\hat{H}^{\mathbf{K}}_{BM}\left(p_x,p_y-\frac{eB}{c}x\right)$ defined via Eq. (1) below with an eigenvalue $E_{\mathbf{K},m,k_1,k_2}$, then $-i\mu_y\sigma_xe^{-i\mathbf{q}_1\cdot\mathbf{r}}\Psi_{\mathbf{K},m,k_1,k_2}(\mathbf{r})$ is an opposite valley eigenstate of $\hat{H}^{\mathbf{K}'}_{BM}\left(p_x,p_y-\frac{eB}{c}x\right)$ with an eigenvalue $-E_{\mathbf{K},m,k_1,k_2}$. The Pauli matrices σ and μ act in the sub-

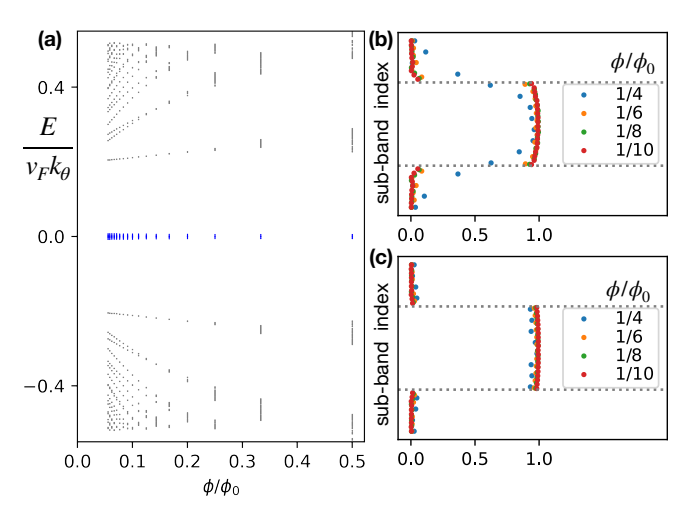


FIG. 2. (a) Hofstadter spectrum for the non-interacting BM Hamiltonian $\hat{H}_{BM}^{\mathbf{K}}(p_x,p_y-\frac{eB}{c}x)$ calculated using Landau level basis at magic angle $w_1/v_Fk_\theta=0.586$ [44] and $w_0/w_1=0.7$. The horizontal axes in (b) and (c) are the overlaps between the $\mathbf{B}=0$ narrow bands hybrid Wannier states projected onto the $\mathbf{B}\neq 0$ representation of the MTG $|V_a\rangle$, and the exact magnetic subband states at various energies obtained using the LL basis $\sum_a |\langle \Psi_{\mathbf{K},m}(k_1,k_2)|V_{\mathbf{K},a}(k_1,k_2)\rangle|^2$; the vertical axes are the sub-band index m. The states in between the dashed lines belong to the $\mathbf{B}\neq 0$ narrow bands shown as blue in (a), demonstrating that at low $\mathbf{B}, |V_a\rangle$ have support almost exclusively within the $\mathbf{B}\neq 0$ narrow band Hilbert space. $w_0/w_1=0.7$ in (b) and (c) is at the chiral limit $w_0/w_1=0$.

lattice and layer spaces, respectively. Eliminating the remote magnetic sub-bands using the RG procedure introduced in Ref. [39] therefore still results in the residual Coulomb interaction projected onto the $\mathbf{B} \neq 0$ narrow band Hilbert space to be of the form expressed in Eq. (7). Moreover, ignoring the Zeeman effect, C_2P guarantees that the spin valley U(4) symmetry [24, 41–43] is still present even at $\mathbf{B} \neq 0$. We can therefore follow the double commutator method outlined in Refs. [39, 40] in order to find the spectrum of the single particle or single hole excitations at $\mathbf{B} \neq 0$. The solutions of the Eq. (9) for two-gate screened Coulomb interaction, $V_{\mathbf{q}} = \frac{2\pi e^2}{\epsilon |\mathbf{q}|} \tanh\left(\frac{|\mathbf{q}|\xi}{2}\right)$, with the gate separation $\xi = L_m$ are shown in the Fig. 3 for the charge neutral point (CNP, i.e. $\nu = 0$), together with their $\mathbf{B} = 0$ density of states. The results at $|\nu|=2$ for the heavy and light mass sides are shown in the Fig.4. Below we provide details of the calculations which lead to the stated results.

To obtain the narrow band Hilbert space, we start by considering the BM model at $\mathbf{B} \neq 0$ in Landau gauge at $\mathbf{B} \neq 0$ in Landau gauge $\hat{H}_{BM}^{\mathbf{K}}\left(p_{x},p_{y}-\frac{eB}{c}x\right)$ where at the valley \mathbf{K}

$$\hat{H}_{BM}^{\mathbf{K}}(p_x, p_y) = \begin{pmatrix} v_F \boldsymbol{\sigma} \cdot \mathbf{p} & T(\mathbf{r})e^{i\mathbf{q}_1 \cdot \mathbf{r}} \\ e^{-i\mathbf{q}_1 \cdot \mathbf{r}}T^{\dagger}(\mathbf{r}) & v_F \boldsymbol{\sigma} \cdot (\mathbf{p} + \hbar \mathbf{q}_1) \end{pmatrix} . (1)$$

The Hamiltonian in valley \mathbf{K}' can be obtained by first applying time reversal to $\hat{H}^{\mathbf{K}}_{BM}(p_x,p_y)$ followed by the minimal substitution $p_y \to p_y - \frac{eB}{c}x$. The Pauli matrices σ act in the sublattice space [45]. The interlayer hopping functions are $T(\mathbf{r}) = \sum_{j=1}^3 T_j e^{-i\mathbf{q}_j \cdot \mathbf{r}}$ where $\mathbf{q}_1 = k_\theta(0,-1)$, $\mathbf{q}_{2,3} = k_\theta \left(\pm \frac{\sqrt{3}}{2}, \frac{1}{2}\right)$, $k_\theta = \frac{8\pi}{3a_0} \sin \frac{\theta}{2} = 4\pi/(3L_m)$, $a_0 \approx 0.246$ nm, L_m is the period of the moiré lattice, and $T_{j+1} = w_0 \mathbf{1}_2 + w_1 \left(\cos \left(\frac{2\pi}{3}j\right)\sigma_x + \sin \left(\frac{2\pi}{3}j\right)\sigma_y\right)$, where $\mathbf{1}_n$ is an $n \times n$ unit matrix. At $\mathbf{B} = 0$, $\hat{H}^{\mathbf{K}}_{BM}$ is invariant under discrete translations by any integer multiple of $\mathbf{L}_1 = L_m \left(\frac{\sqrt{3}}{2}, \frac{1}{2}\right)$ and $\mathbf{L}_2 = L_m(0,1)$. At $\mathbf{B} \neq 0$ and in the chosen gauge $\hat{H}^{\mathbf{K}}_{BM}$ is still invariant under the translation by \mathbf{L}_2 , but a translation by \mathbf{L}_1 needs to be accompanied by a gauge transformation,

$$\psi(\mathbf{r}) \to \hat{t}_{\mathbf{L}_1} \psi(\mathbf{r}) = e^{i\frac{eB}{\hbar c} L_{1x} y} \psi(\mathbf{r} - \mathbf{L}_1).$$
 (2)

Thus, if $\psi(\mathbf{r})$ is an eigenstate then so is $e^{i\frac{eB}{\hbar c}L_{1x}y}\psi(\mathbf{r}-\mathbf{L}_1)$. Translations by \mathbf{L}_2 are generated by $\hat{t}_{\mathbf{L}_2}\psi(\mathbf{r})=\psi(\mathbf{r}-\mathbf{L}_2)$. Then $\hat{t}_{\mathbf{L}_2}\hat{t}_{\mathbf{L}_1}=e^{-2\pi i\phi/\phi_0}\hat{t}_{\mathbf{L}_1}\hat{t}_{\mathbf{L}_2}$, where $\phi_0=\frac{\hbar c}{e}$ and $\phi=BL_{1x}L_m$. If $\phi/\phi_0=p/q$, with p and q relatively prime integers, then $[\hat{t}_{\mathbf{L}_2}^q,\hat{t}_{\mathbf{L}_1}]=0$.

The $\mathbf{B} = 0$ hWSs, $|w_{\pm}(n, k\mathbf{g}_2)\rangle$, can be chosen to be eigenstates of the periodic position operator $\hat{O} = \hat{P}e^{-i\frac{1}{N_1}\mathbf{g}_1\cdot\mathbf{r}}\hat{P}$, projected using \hat{P} onto the $\mathbf{B} = 0$ narrow band Hilbert space studied (for details see Ref.[33]); here N_1 is a large integer. The eigenvalues $e^{-2\pi i\frac{1}{N_1}(n+\langle x_{\pm}\rangle_k/|\mathbf{L}_1|)}$ give the Wilson loops [27, 32–34] for the Chern +1 and Chern -1 hWSs. These states are localized along \mathbf{L}_1 and Bloch extended along \mathbf{L}_2 , as illustrated in the Fig. 1 As shown in Ref. [33], they satisfy,

$$\hat{t}_{\mathbf{L}_1}|w_{\pm}(n, k_2\mathbf{g}_2)\rangle = e^{i\frac{eB}{\hbar c}L_{1x}y}|w_{\pm}(n+1, k_2\mathbf{g}_2)\rangle$$
(3)

$$\hat{t}_{\mathbf{L}_2}|w_{\pm}(n, k_2\mathbf{g}_2)\rangle = e^{-2\pi i k_2}|w_{\pm}(n, k_2\mathbf{g}_2)\rangle.$$
(4)

We construct our basis for the narrow band at $\mathbf{B} \neq 0$ by projecting $|w_{\pm}(n_0, k_2\mathbf{g}_2)\rangle$ onto representation of the MTG. We include in our set a range of n_0 's near 0 as

$$|W_{\pm}(k_1, k_2; n_0)\rangle = \frac{1}{\sqrt{N}} \sum_{s=-\infty}^{\infty} e^{2\pi i s k_1} \hat{t}_{\mathbf{L}_1}^{s} |w_{\pm}(n_0, k_2 \mathbf{g}_2)\rangle,$$
(5)

with normalization factor N and for $k_1 \in [0,1)$ and temporarily letting $k_2 \in [0,1)$. The results in Figs.2b, 2c and 3 include $n_0 = 0$ and 1. Note that $|W_{\pm}(k_1, k_2; n_0)\rangle$ are simultaneous eigenstates of $\hat{t}_{\mathbf{L}_1}$ and $\hat{t}_{\mathbf{L}_2}^q$ with eigenvalues $e^{-2\pi i k_1}$ and $e^{-2\pi i q k_2}$, respectively. Thus the $q\mathbf{L}_2$ translations break up the k_2 domain into q pieces of equal width 1/q. Therefore, we let $|W_{\pm}(k_1, k_2 + l/q; n_0)\rangle$, permanently fix $k_2 \in [0, 1/q)$, and let $l = 0, 1, \ldots, q - 1$. For different values of k_1 and k_2 in their respective domains $|W_{\pm}(k_1, k_2 + l/q; n_0)\rangle$'s are orthogonal because they have different eigenvalues under $\hat{t}_{\mathbf{L}_1}$ and $\hat{t}_{\mathbf{L}_2}^q$. For the same k_1 and k_2 , but different l (and different n_0) the

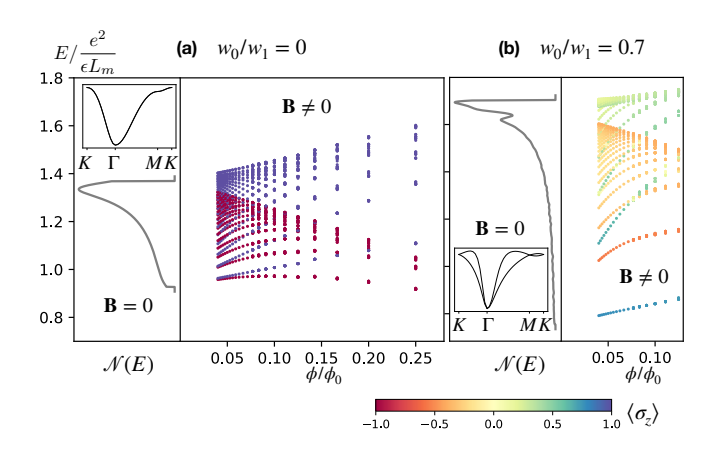


FIG. 3. Landau level spectrum at magic angle in the strong coupling limit for (a) $w_0/w_1 = 0$ and (b) $w_0/w_1 = 0.7$. The gray lines denote the respective density of states $\mathcal{N}(E)$ at $\mathbf{B} = 0$, and the color of each magnetic sub-band denotes the average value of its sublattice polarization. Blue (red) denotes purely A (B) sublattice polarization.

states $|W_{\pm}(k_1, k_2 + l/q; n_0)\rangle$'s are in general not orthogonal. To orthogonalize them we diagonalize the overlap matrix $M_{ab} = \langle W_a | W_b \rangle = (U^{\dagger}DU)_{ab}$ where D is diagonal. In the above we combined l, the Chern number index $c = \pm$, and n_0 into a single index a for each k_1 and k_2 , whose dependence we temporarily suppress. Then we let

$$|V_a\rangle = \sum_b |W_b\rangle U_{ba}^{\dagger} \frac{1}{\sqrt{D_a}} \tag{6}$$

where b runs over all the indices but a runs only over the 2q largest eigenvalues D_a . As demonstrated in Fig. 2b and Fig. 2c, at low \mathbf{B} , the 2q orthogonal states $|V_a(k_1,k_2)\rangle$ at each k_1 and k_2 now form the basis spanning almost exclusively only the $\mathbf{B} \neq 0$ narrow bands. At larger \mathbf{B} , we find a spillover into the remote bands; for the results presented the spillover is negligible.

Having constructed the $\mathbf{B} \neq 0$ narrow band Hilbert space from the non-interacting BM model, we proceed to study the spectrum of charged excitations in the strong coupling limit at integer fillings of $\nu=0$ and $|\nu|=2$, where the ground states at $\mathbf{B}=\mathbf{0}$ have been shown to be correlated insulating states belonging to the U(4) manifold [46], and the spectrum of charged excitations is entirely due to the Coulomb interaction projected onto the narrow band Hilbert space. In this case the Hamiltonian consists of only the interaction $V(\mathbf{r}-\mathbf{r}')$ projected onto the $\mathbf{B} \neq 0$ narrow band basis. As described earlier, the C_2P symmetry guarantees that the dominant term takes the form

$$\hat{H}_{int} = \frac{1}{2} \int d\mathbf{r} \int d\mathbf{r}' V(\mathbf{r} - \mathbf{r}') \delta \rho(\mathbf{r}) \delta \rho(\mathbf{r}'), \qquad (7)$$

where $\delta \rho(\mathbf{r}) = \rho(\mathbf{r}) - \bar{\rho}(\mathbf{r})$. Restoring the indices on our $\mathbf{B} \neq 0$ narrow band basis functions $\langle \mathbf{r} | V_a \rangle$, the projected

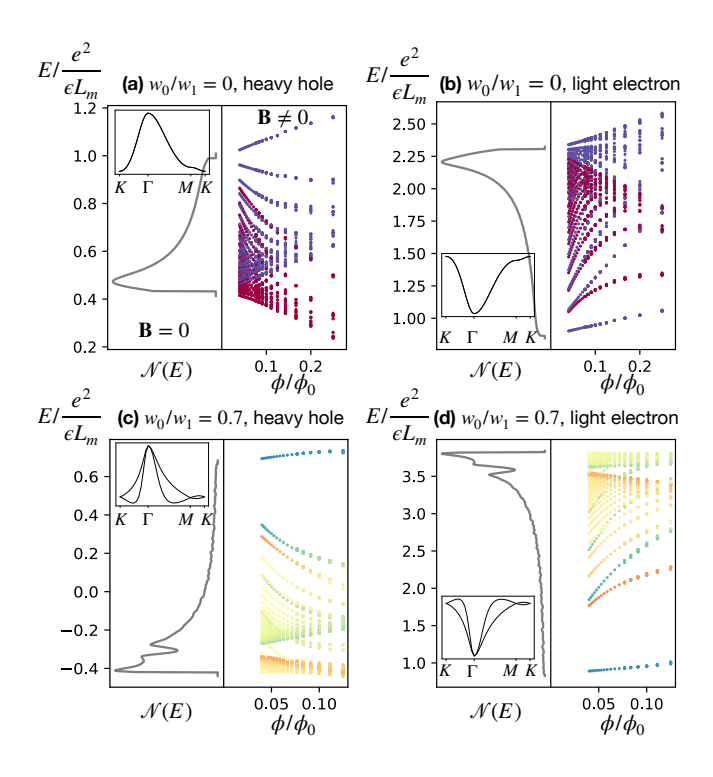


FIG. 4. Landau level spectrum of charge ± 1 excitations at $|\nu|=2$ at magic angle in the strong coupling limit. Heavy hole (a,c) and light electron (b,d) excitations for $w_0/w_1=0$ and $w_0/w_1=0.7$ respectively [40, 46]. The color scale for sublattice polarization is the same as in Fig. 3.

density operator is $\rho(\mathbf{r}) =$

$$\sum_{k_1,k_2,a} \sum_{k_1',k_2',a'} V_{\mathbf{K},a}^{\dagger}(k_1,k_2;\mathbf{r}) V_{\mathbf{K},a'}(k_1',k_2';\mathbf{r}) \mathfrak{d}_{a,k_1,k_2}^{\dagger} \mathfrak{d}_{a',k_1',k_2'}.$$

We arranged the fermion creation operators with 2q discrete quantum numbers a and momentum k_1,k_2 into 4-component "spinor", $\mathfrak{d}^{\dagger}_{a,k_1,k_2} = \begin{pmatrix} d^{\dagger}_{\uparrow,\mathbf{K};a,k_1,k_2}, d^{\dagger}_{\downarrow,\mathbf{K};a,k_1,k_2}, d^{\dagger}_{\uparrow,\mathbf{K}';C_2P[a,k_1,k_2]}, d^{\dagger}_{\downarrow,\mathbf{K}';C_2P[a,k_1,k_2]} \end{pmatrix}$. The U(4) manifold can be generated from a valley polarized state, which is an eigenstate of $\rho(\mathbf{r})$ with the eigenvalue equal to $\bar{\rho}(\mathbf{r})$ at CNP, where it takes the form, say, $|\Phi_{\nu=0}\rangle = \prod_{a,k_1,k_2,\sigma=\uparrow,\downarrow} d^{\dagger}_{\sigma,\mathbf{K};a,k_1,k_2}|0\rangle$. Excitations can be created using an operator X (see Ref. [39]) and their strong coupling eigenenergies can be read off from the equation

$$EX|\Phi_{\nu}\rangle = \frac{1}{2} \int d^{2}\mathbf{r} d^{2}\mathbf{r}' V(\mathbf{r} - \mathbf{r}') \left[\rho(\mathbf{r}), \left[\rho(\mathbf{r}'), X\right]\right] |\Phi_{\nu}\rangle$$
$$+ \int d^{2}\mathbf{r} d^{2}\mathbf{r}' V(\mathbf{r} - \mathbf{r}') \left[\rho(\mathbf{r}), X\right] \delta \bar{\rho}(\mathbf{r}') |\Phi_{\nu}\rangle, \quad (9)$$

where we extended the result to include $\nu=\pm 2$ fillings [40, 46]; the valley polarized states $|\Phi_{\nu}\rangle$ are eigenstates of $\delta\rho(\mathbf{r})$ with an eigenvalue $\delta\bar{\rho}(\mathbf{r})$ [47]. The eigenenergies of the strong coupling single particle or single hole excitations can now be determined from diagonalizing a

 $2q \times 2q$ matrix for each k_1 and k_2 . Their degeneracy is determined by considering the action of X on $|\Phi_{\nu}\rangle$.

The resulting spectra at CNP are shown in the right panel of Fig. 3a for the chiral limit $w_0/w_1=0$ and the right panel of Fig. 3b for $w_0/w_1 = 0.7$; the spectra at $|\nu|=2$ are shown in Fig. 4. We clearly see that despite being at strong coupling the excitations' spectra are Landau quantized in $\mathbf{B} \neq 0$. In the chiral limit (Fig. 3a), the degeneracy of the low lying excitations limits to 4 at low B due to spin and sublattice degrees of freedom, the latter taking on values ± 1 as marked by the blue and red colors. Because they originate from $\mathbf{B} = 0$ Chern bands with opposite total Chern numbers, the B sublattice sector has q-1 sub-bands while the A sublattice sector has q+1 sub-bands for the 1/q sequence shown. Note that at small \mathbf{B} there is a small splitting between the low lying opposite sublattice polarized strong coupling sub-bands due to broken C_2T symmetry and that this splitting increases with increasing **B**. A similar conclusion has been reached in a recent theoretical work [24], which reported energy splitting of the charge- ± 1 excitations at full flux $\phi/\phi_0 = 1$. Also note the opposite evolution of the subbands emanating from the $\mathbf{B} = 0$ van Hove singularities. Many of the features are reproduced at $w_0/w_1 = 0.7$, except the smaller mean value of the sublattice polarization (as marked by the color scheme), and larger splitting between the low lying magnetic sub-bands. Interestingly, the sizable splitting between the light fermion LLs seen for $w_0/w_1 = 0.7$ in Figs. 3b and 4d even at small ϕ/ϕ_0 would give rise to prominent LL filling factors $|\nu_{LL}| = 0, 2$ at CNP, and $\nu_{LL} = 0, 1$ on the light mass side of $\nu = 2$, as observed in Ref. [15] without invoking moiré translational symmetry breaking.

SQUID-on-tip measurements found large orbital magnetic moments near $\nu=3$ [48] and $\nu=1$ [49]. We calculate the total energy cost per moiré unit cell to fully fill the Chern +1 and Chern -1 magnetic subbands in the chiral limit along the $\phi/\phi_0=1/q$ sequence, defined as $E_{\pm}=\frac{1}{q}\frac{1}{N}\sum_{\mathbf{k}}\sum_{i=1}^{q\pm 1}\varepsilon_{i,\mathbf{k}}$. Here $\mathbf{k}\in[0,1)\times[0,1/q)$, and N is the total number of \mathbf{k} points in the discrete sum. $\varepsilon_{i,\mathbf{k}}$ are the eigenenergies shown in Figs. (3) and (4). We find that at $\nu=0$ and $|\nu|=2$, $E_{\pm}\approx E_0(\nu)\pm g\mu_B B$ (see SM Sec.IV), where $\mu_B=\frac{e\hbar}{2mc}$ is the Bohr magneton, and $g\approx\frac{\sqrt{3}}{\pi}\frac{mL_m^2}{\hbar^2}\frac{e^2}{\epsilon L_m}$. Taking $\frac{e^2}{\epsilon L_m}=10$ meV gives $g\approx 13.4$ at the magic angle, which is within the range of experimental values [48, 49].

STM data [50] at $\mathbf{B} \neq 0$ show only results from regions with the values of heterostrain 0.1% - 0.4%. It is known that even such small values of strain dramatically increase the non-interacting narrow band width [51, 52], making the kinetic energy comparable or larger than the Coulomb interaction scale $e^2/\epsilon L_m$, and stabilizing energetically proximate nematic state [33, 52, 53]. Therefore, the available STM data [50] at $\mathbf{B} \neq 0$ may not be in the limit dominated by the Coulomb interaction complicat-

ing the comparison with the our result. Measurements on magic angle devices at $\mathbf{B} \neq 0$ with negligible strain would be highly desirable.

Our method is general, and can be used to find the Hofstadter spectrum at larger ϕ/ϕ_0 by starting with simple fractions $1/\bar{q}$, where $\bar{q}=1,2$ or 3, where the LL based calculation is manageable, building the hWSs for the $2\bar{q}$ Hofstadter bands, and then projecting onto the representation of the MTG for ϕ/ϕ_0 away from $1/\bar{q}$ (See SM Sec.III.D for a brief discussion). Such generalizations, as well as strain effects will be presented in future work.

We thank B. Andrei Bernevig, Jonah Herzog-Arbeitman, Jian Kang, Mike Zaletel for helpful discussions. X.W. acknowledges financial support from National MagLab through Dirac fellowship, which is funded by the National Science Foundation (Grant No. DMR-1644779) and the state of Florida. O.V. was supported by NSF Grant No. DMR-1916958.

* vafek@magnet.fsu.edu

- [1] Y. Cao, V. Fatemi, A. Demir, S. Fang, S. L. Tomarken, J. Y. Luo, J. D. Sanchez-Yamagishi, K. Watanabe, T. Taniguchi, E. Kaxiras, R. C. Ashoori, and P. Jarillo-Herrero, Nature 556, 80 (2018).
- [2] Y. Cao, V. Fatemi, S. Fang, K. Watanabe, T. Taniguchi, E. Kaxiras, and P. Jarillo-Herrero, Nature 556, 43 (2018).
- [3] A. Kerelsky, L. J. McGilly, D. M. Kennes, L. Xian, M. Yankowitz, S. Chen, K. Watanabe, T. Taniguchi, J. Hone, C. Dean, A. Rubio, and A. N. Pasupathy, Nature 572, 95 (2019).
- [4] X. Lu, P. Stepanov, W. Yang, M. Xie, M. A. Aamir, I. Das, C. Urgell, K. Watanabe, T. Taniguchi, G. Zhang, A. Bachtold, A. H. MacDonald, and D. K. Efetov, Nature 574, 653 (2019).
- [5] Y. Jiang, X. Lai, K. Watanabe, T. Taniguchi, K. Haule, J. Mao, and E. Y. Andrei, Nature 573, 91 (2019).
- [6] M. Yankowitz, S. Chen, H. Polshyn, Y. Zhang, K. Watanabe, T. Taniguchi, D. Graf, A. F. Young, and C. R. Dean, Science 363, 1059 (2019).
- [7] Y. Choi, J. Kemmer, Y. Peng, A. Thomson, H. Arora, R. Polski, Y. Zhang, H. Ren, J. Alicea, G. Refael, F. von Oppen, K. Watanabe, T. Taniguchi, and S. Nadj-Perge, Nature Physics 15, 1174 (2019).
- [8] A. L. Sharpe, E. J. Fox, A. W. Barnard, J. Finney, K. Watanabe, T. Taniguchi, M. A. Kastner, and D. Goldhaber-Gordon, Science 365, 605 (2019).
- [9] Y. Xie, B. Lian, B. Jäck, X. Liu, C.-L. Chiu, K. Watanabe, T. Taniguchi, B. A. Bernevig, and A. Yazdani, Nature 572, 101 (2019).
- [10] U. Zondiner, A. Rozen, D. Rodan-Legrain, Y. Cao, R. Queiroz, T. Taniguchi, K. Watanabe, Y. Oreg, F. von Oppen, A. Stern, E. Berg, P. Jarillo-Herrero, and S. Ilani, Nature 582, 203 (2020).
- [11] D. Wong, K. P. Nuckolls, M. Oh, B. Lian, Y. Xie, S. Jeon, K. Watanabe, T. Taniguchi, B. A. Bernevig, and A. Yazdani, Nature 582, 198 (2020).
- [12] M. Serlin, C. L. Tschirhart, H. Polshyn, Y. Zhang, J. Zhu,

- K. Watanabe, T. Taniguchi, L. Balents, and A. F. Young, Science **367**, 900 (2020).
- [13] P. Stepanov, I. Das, X. Lu, A. Fahimniya, K. Watanabe, T. Taniguchi, F. H. L. Koppens, J. Lischner, L. Levitov, and D. K. Efetov, Nature 583, 375 (2020).
- [14] X. Liu, Z. Wang, K. Watanabe, T. Taniguchi, O. Vafek, and J. I. A. Li, Science 371, 1261 (2021).
- [15] A. T. Pierce, Y. Xie, J. M. Park, E. Khalaf, S. H. Lee, Y. Cao, D. E. Parker, P. R. Forrester, S. Chen, K. Watanabe, T. Taniguchi, A. Vishwanath, P. Jarillo-Herrero, and A. Yacoby, Nature Physics 17, 1210 (2021).
- [16] S. Wu, Z. Zhang, K. Watanabe, T. Taniguchi, and E. Y. Andrei, Nature Materials 20, 488 (2021).
- [17] R. Bistritzer and A. H. MacDonald, Phys. Rev. B 84, 035440 (2011).
- [18] P. Moon and M. Koshino, Phys. Rev. B 90, 155406 (2014).
- [19] K. Hejazi, C. Liu, and L. Balents, Phys. Rev. B 100, 035115 (2019).
- [20] Y.-H. Zhang, H. C. Po, and T. Senthil, Phys. Rev. B 100, 125104 (2019).
- [21] B. Andrews and A. Soluyanov, Phys. Rev. B 101, 235312 (2020).
- [22] B. Lian, F. Xie, and B. A. Bernevig, Phys. Rev. B 102, 041402 (2020).
- [23] J. Herzog-Arbeitman, Z.-D. Song, N. Regnault, and B. A. Bernevig, Phys. Rev. Lett. 125, 236804 (2020).
- [24] J. Herzog-Arbeitman, A. Chew, D. K. Efetov, and B. A. Bernevig, (2021), arXiv:2111.11434.
- [25] H. C. Po, L. Zou, A. Vishwanath, and T. Senthil, Phys. Rev. X 8, 031089 (2018).
- [26] J. Ahn, S. Park, and B.-J. Yang, Phys. Rev. X 9, 021013 (2019).
- [27] Z. Song, Z. Wang, W. Shi, G. Li, C. Fang, and B. A. Bernevig, Phys. Rev. Lett. 123, 036401 (2019).
- [28] C. R. Dean, L. Wang, P. Maher, C. Forsythe, F. Ghahari, Y. Gao, J. Katoch, M. Ishigami, P. Moon, M. Koshino, T. Taniguchi, K. Watanabe, K. L. Shepard, J. Hone, and P. Kim, Nature 497, 598 (2013).
- [29] Y. Saito, J. Ge, L. Rademaker, K. Watanabe, T. Taniguchi, D. A. Abanin, and A. F. Young, Nature Physics 17, 478 (2021).
- [30] J. Finney, A. L. Sharpe, E. J. Fox, C. L. Hsueh, D. E. Parker, M. Yankowitz, S. Chen, K. Watanabe, T. Taniguchi, C. R. Dean, A. Vishwanath, M. Kastner, and D. Goldhaber-Gordon, (2021), arXiv:2105.01870.
- [31] R. Bistritzer and A. H. MacDonald, Proceedings of the National Academy of Sciences 108, 12233 (2011).
- [32] R. Yu, X. L. Qi, A. Bernevig, Z. Fang, and X. Dai, Phys. Rev. B 84, 075119 (2011).
- [33] J. Kang and O. Vafek, Phys. Rev. B 102, 035161 (2020).
- [34] T. Soejima, D. E. Parker, N. Bultinck, J. Hauschild, and M. P. Zaletel, Phys. Rev. B 102, 205111 (2020).
- [35] In Supplemental Material we provide a derivation of p anomalous magnetic sub-bands at flux p/q in the chiral limit based on the tripod model of Ref. [54], and provide numerical evidence both in and away from the chiral limit.
- [36] O. Vafek and A. Melikyan, Phys. Rev. Lett. 96, 167005 (2006).
- [37] F. K. Popov and A. Milekhin, Phys. Rev. B 103, 155150 (2021).
- [38] Y. Sheffer and A. Stern, Phys. Rev. B 104, L121405 (2021).

- [39] O. Vafek and J. Kang, Phys. Rev. Lett. 125, 257602 (2020).
- [40] B. A. Bernevig, B. Lian, A. Cowsik, F. Xie, N. Regnault, and Z.-D. Song, Phys. Rev. B 103, 205415 (2021).
- [41] J. Kang and O. Vafek, Phys. Rev. Lett. 122, 246401 (2019).
- [42] N. Bultinck, E. Khalaf, S. Liu, S. Chatterjee, A. Vishwanath, and M. P. Zaletel, Phys. Rev. X 10, 031034 (2020).
- [43] B. A. Bernevig, Z.-D. Song, N. Regnault, and B. Lian, Phys. Rev. B 103, 205413 (2021).
- [44] G. Tarnopolsky, A. J. Kruchkov, and A. Vishwanath, Phys. Rev. Lett. 122, 106405 (2019).
- [45] We ignore the small rotation of σ matrices which was shown to lead to negligible effects on the narrow band Hilbert space.
- [46] J. Kang, B. A. Bernevig, and O. Vafek, Phys. Rev. Lett. 127, 266402 (2021).
- [47] B. Lian, Z.-D. Song, N. Regnault, D. K. Efetov, A. Yaz-dani, and B. A. Bernevig, Phys. Rev. B 103, 205414 (2021).

- [48] C. L. Tschirhart, M. Serlin, H. Polshyn, A. Shragai, Z. Xia, J. Zhu, Y. Zhang, K. Watanabe, T. Taniguchi, M. E. Huber, and A. F. Young, Science 372, 1323 (2021).
- [49] S. Grover, M. Bocarsly, A. Uri, P. Stepanov, G. D. Battista, I. Roy, J. Xiao, A. Y. Meltzer, Y. Myasoedov, K. Pareek, K. Watanabe, T. Taniguchi, B. Yan, A. Stern, E. Berg, D. K. Efetov, and E. Zeldov, Imaging chern mosaic and berry-curvature magnetism in magic-angle graphene (2022), arXiv:2201.06901.
- [50] K. P. Nuckolls, M. Oh, D. Wong, B. Lian, K. Watanabe, T. Taniguchi, B. A. Bernevig, and A. Yazdani, Nature 588, 610 (2020).
- [51] Z. Bi, N. F. Q. Yuan, and L. Fu, Phys. Rev. B 100, 035448 (2019).
- [52] D. E. Parker, T. Soejima, J. Hauschild, M. P. Zaletel, and N. Bultinck, Phys. Rev. Lett. 127, 027601 (2021).
- [53] S. Liu, E. Khalaf, J. Y. Lee, and A. Vishwanath, Phys. Rev. Research 3, 013033 (2021).
- [54] B. A. Bernevig, Z.-D. Song, N. Regnault, and B. Lian, Phys. Rev. B 103, 205411 (2021).